3. Force Calibration

3.1 Introduction

In this chapter we consider a number of specific issues related to the calibration of force measurements using friction force microscopy (FFM). As discussed previously, the FFM can provide information on the atomic-level frictional properties of surfaces. However, reproducible quantitative measurements are in fact difficult to obtain for reasons we shall discuss below.

The most common experimental apparatus for FFM combines commercially available microfabricated silicon or silicon nitride cantilever-tip assemblies with an AFM using optical beam deflection sensing[1,2]. All commercially available scanning probe microscopes capable of FFM and many custom designed instruments use this combination[3,4].

Microfabricated cantilevers offer many advantages - they are available in a range of force constants, their small size leads to high resonant frequencies, they are relatively easy to use, and the tips are relatively sharp and durable. On the other hand, their small size makes it difficult to make direct measurements of mechanical properties such as the force constants of the cantilever. Calculation of cantilever force constants are also difficult as they depend on knowledge of critical dimensions such as lever thickness and tip height that are difficult to control in fabrication and difficult to measure accurately even with a good scanning electron microscope (SEM). The mechanical properties of silicon nitride cantilevers produced by chemical vapor deposition (CVD) can vary widely[5,6]. Levers are often metalized to increase optical reflectivity, but the thickness and mechanical properties of the

coating (grain size, etc.) may not be known and the effect of metalization on the cantilever force constants can be significant[7]. In general, calculations for the commonly used V-shaped levers require complex numerical methods[8,9].

The optical beam deflection sensor also has experimental advantages for FFM along with difficulties for quantitative friction measurements. One sensor can measure deflections due to both normal and lateral forces. The sensitivity and signal/noise ratio of this method are good and changing cantilevers is relatively easy. However, both the absolute values and the *ratio* of normal and lateral force sensitivity depends on the precise alignment of the laser beam with respect to the cantilever. Furthermore, the angular deflection of commercial cantilevers due to lateral forces is one to two orders of magnitude smaller than for normal forces, so small misalignments can cause significant errors in lateral force measurement due to cross-talk between normal and lateral deflections.

In general, discussion or even statements of uncertainties in AFM measurements is often neglected. A good introduction to aspects of error analysis with force microscopy is contained in the paper of Schwarz *et al.*[10] Here we will discuss some experimental aspects of the optical deflection FFM, present methods for estimating the normal and lateral response of microfabricated cantilevers, describe the "wedge" method of force calibration, and present experimental results for commercial V-shape cantilevers[11].

3.2 Optical Beam FFM

In the optical beam deflection method, a laser beam is reflected off the back of the AFM cantilever into a quadrant photodiode position sensitive detector. We define a coordinate system with *X* along the lever long axis, *Z* along the tip axis, and the origin at the base of the lever. The incident laser beam is in the *X-Z* plane, and the reflected beam is incident on a four-quadrant photodiode which is (ideally) oriented with one axis along the *Y* direction in the *X-Z* plane (Figure 3.1). For small deflections the difference in photocurrent between the upper and lower pairs of diodes (*A-B*) will be proportional to the slope of the

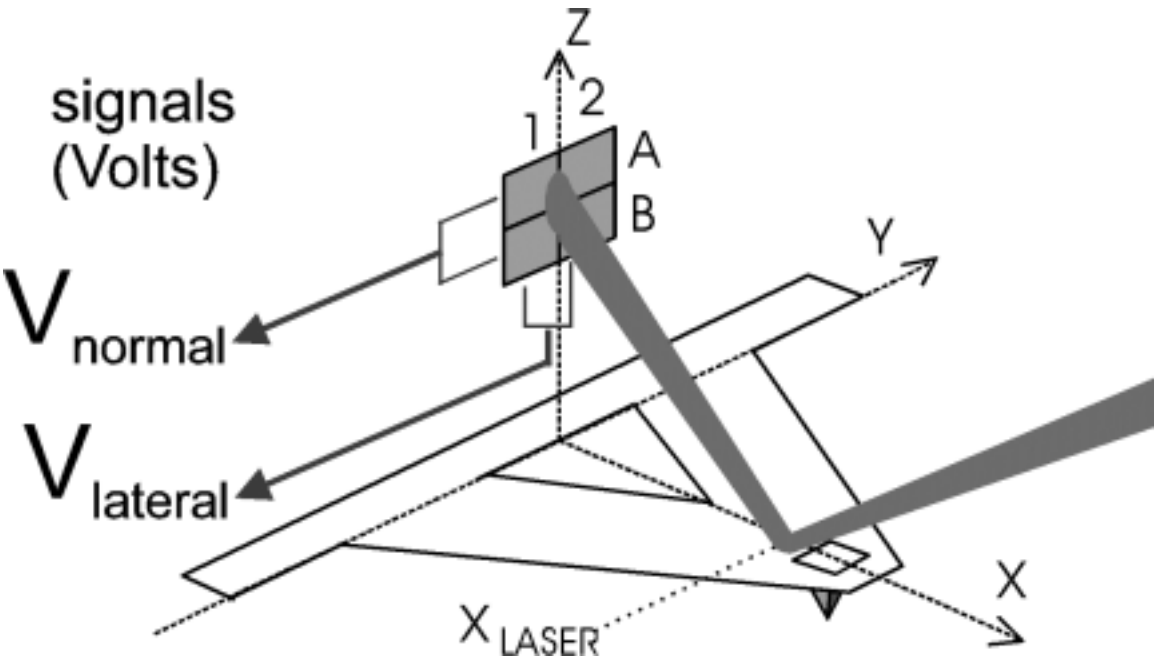

Figure 3.1 Schematic of cantilever and deflection sensor for the optical beam deflection FFM. The incident laser beam in the X-Z plane is deflected proportional to the slope (not the displacement) of the lever X-Z plane, and to the twist of the lever normal out of this plane, at the point where the laser beam hits the lever.

lever in the *X-Z* plane at the point of reflection X_{LASER}. Similarly, the difference in photocurrent between the left and right pairs of diodes (*1-2*) is proportional to the lever twist out of the *X*-Z plane at X_{LASER}.

The photodiode output signal *S* as a function of angular deflection φ can be calculated for a Gaussian beam if the total size of the photodiode is large compared to the laser spot and the "dead" area between the quadrants is neglected. In this case

$$S(\varphi) = \frac{A-B}{A+B} = 1 - \frac{1}{\Delta\omega}\sqrt{\frac{8}{\pi}}\int_{\varphi}^{\infty} e^{\frac{-2u^2}{\Delta\omega^2}}\,du \qquad (3.1)$$

where $\Delta\omega$ is the Gaussian half width (angular divergence) of the beam, *A* is the photocurrent on the upper two quadrants, and *B* is the photocurrent on the lower two quadrants. This

expression cannot be integrated analytically, but it may be expanded around $\varphi = 0$ (see appendix), with $x = \frac{\varphi}{\Delta\omega}$

$$S(x) = \sqrt{\tfrac{8}{\pi}}x[1 - \tfrac{2}{3}x^2 + \tfrac{2}{5}x^4 - \tfrac{4}{21}x^6 + ...] \qquad (3.2)$$

The term in square brackets describes the non-linearity of the detector response. For $S = 0.2$, the deviation from linearity is -1% and for $S = 0.5$ it is -6.1%. Under our typical experimental conditions, a normal force of ~ 1 nN produces a deflection $S \sim 0.002$. The photodiode detector signal is quite linear in response to FFM lever deflection over a relatively wide range, which we have verified experimentally using a laser interferometer to independently monitor microscope displacement.

If the reflected laser beam is round, the angular sensitivity is equal for deflections due to normal and lateral forces. This is often not the case under experimental conditions. Most optical beam FFMs use diode lasers, which produce asymmetric beams. In addition, if the laser spot is not carefully focused and aligned on the cantilever, there may be significant diffraction effects where the reflected spot is cut off by the cantilever edge. Let

$$R_{DETECTOR} = \frac{dS_{NORMAL}}{d\vartheta} \Big/ \frac{dS_{LATERAL}}{d\phi} \qquad (3.3)$$

describe the angular sensitivity ratio for normal and lateral angular deflections. If the beam is focused on the cantilever through a single-mode optical fiber, it is possible to have a radially symmetric and well focused Gaussian beam incident on the cantilever. In this case $R_{DETECTOR}$ can be very near 1.

Forces acting on the apex of the tip in the Z direction cause the lever to bend with a displacement z and tip spring constant k_Z of the form

$$z(F_Z, x) = F_Z f(x) \qquad (3.4)$$

$$k_Z = 1 / f(X_{TIP}) \tag{3.5}$$

with the tip located at X_{TIP}. Microfabricated levers are generally planar, and quite stiff with respect to bending in the *X*-*Y* plane, and in any case such deformations cannot be detected by the optical beam method. The main effect of lateral forces (acting on the tip apex in the *Y* direction) is to twist the lever, with an angular deflection Θ and resulting tip spring constant k_Y of the form:

$$\Theta(F_Y, x) = F_Y g(x) \tag{3.6}$$

$$k_Y = 1 / H_{TIP} g(X_{TIP}) \tag{3.7}$$

where $\mathcal{H}_{TIP}$ is the cantilever tip height. Longitudinal forces (acting on the tip apex in the *X* direction) are more complicated for the optical beam FFM. The in-plane compression of the lever is insignificant, so the main effect is to cause a bending or buckling of the lever in the *X*-*Z* plane

$$z(F_X) = F_X h(x) \quad . \tag{3.8}$$

The tip displacement Δx and associated spring constant k_X for the tip apex in the *X* direction due to cantilever buckling are

$$\Delta x = F_x H_{TIP} \frac{\partial h(X_{TIP})}{\partial x} \tag{3.9}$$

$$k_X = 1 / H_{TIP} \frac{\partial h(X_{TIP})}{\partial x} \tag{3.10}$$

Bending of the tip itself due to forces in the *X* or *Y* direction will not be detected by the optical beam method. Compression of the tip along its axis (*Z* direction) is insignificant.

We can define a lever deflection sensitivity ratio

$$R_{LEVER}(x) = \frac{\partial f(x)}{\partial x} \Big/ g(x) \tag{3.11}$$

as the ratio of angular deflections produced by normal and lateral forces.

For the "V-shape" cantilevers commonly used in FFM the functions $f(x)$, $g(x)$ and $h(x)$ that describe the lever response must be calculated numerically. Some insight into the general properties of the optical beam method can be gained by considering the form of these functions for a simple beam lever of width $\mathcal{W}_L$ and thickness $\mathcal{T}_L$ which is small compared to its length $\mathcal{L}_L$, with a tip of height $\mathcal{H}_{TIP}$ at the extreme end ($X_{TIP} = \mathcal{L}_L$). Using familiar continuum elasticity theory formulas[12]

$$f(x) = \frac{6L_L x^2 - 2x^3}{EW_L T_L^3} \tag{3.12}$$

$$g(x) = \frac{3H_{TIP} x}{GW_L T_L^3} \tag{3.13}$$

$$h(x) = \frac{6H_{TIP} x^2}{EW_L T_L^3} \tag{3.14}$$

where E and G are the Young's and shear moduli of the cantilever. Notice that these functions do not have the same x dependence - the ratio as well as the absolute values of the angular sensitivities to normal and lateral forces depend on the laser spot position X_{LASER}. For the simple beam

$$R_{LEVER}(x) = \frac{2L_L - x}{H_{TIP}(1+\nu)} \tag{3.15}$$

where

$$G = \frac{E}{2(1+\nu)} \tag{3.16}$$

defines the Poisson ratio ν.

Typical microfabricated cantilevers have tip heights ~ 3 - 4 μm and lengths ~ 80 - 300 μm, so the lateral force signals are ~ 20 to 80 times smaller than the normal force signals. Uncertainty in tip height will cause an error $\Delta R_{LEVER}/R_{LEVER}$ of ~$\Delta H_{TIP}/H_{TIP}$, and uncertainty in laser spot position will cause an error of ~ $X_{LASER} / \mathcal{L}_L$ if the laser spot is near the end of the lever.

3.3 Spring Constant Estimates

An estimate of the response of a "V" lever has been made by treating it as a variable width beam. The curvature of a small solid element is proportional to the moment of torque acting on it and inversely proportional to the product of the elastic modulus and the moment of inertia around the bending axis[12]. Using this approach for the lever, the curvature at a distance x from the base of the lever is

$$\frac{\partial^2 z(x)}{\partial x^2} = \frac{F_Z \cdot (X_{TIP} - x)}{EI(x)} \tag{3.17}$$

where the moment of inertia $I(x) = \frac{1}{12} W_L(x) T_L^{\,3}$ depends on the projected width of the lever along the y axis. Likewise the curvature due to lateral forces is

$$\frac{\partial \Theta(x)}{\partial x} = \frac{F_Y H_{TIP}}{GI(x)} \tag{3.18}$$

These expressions can be integrated analytically for each section and combined, matching boundary conditions for continuity, to give $g(x)$ and $\partial f(x)/\partial x$ along the lever.

This approach is similar to the "parallel beam approximation" (PBA) analyzed in detail by Sader[13]. Warmack *et al.*[14] have also used this type of approach to analyze normal deflections and the effects of cantilever buckling on AFM response. Unlike Sader and references therein, we also calculate torsional and buckling force constants, and explicitly include the effect of the triangular "fillets" (a 10% effect for short levers) in the corners of the central area cut-out of the "V" lever (Figure 3.2). Our approach gives the same result

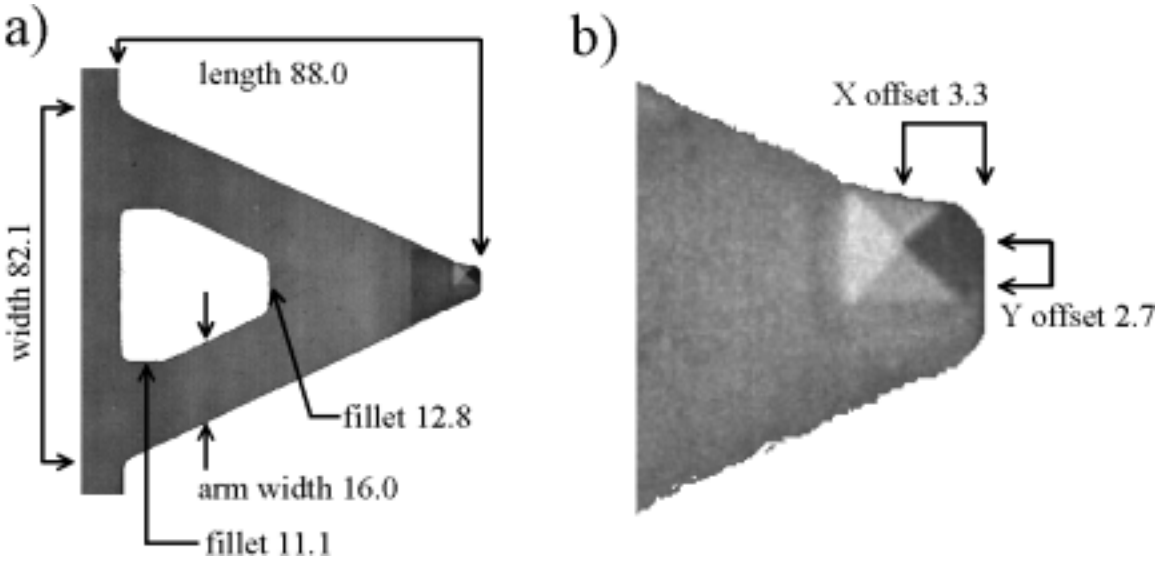

Figure 3.2 (a) A scanning electron micrograph of a gold coated Park Scientific Instruments "F" cantilever. The indicated dimensions are in micrometers. (b) A higher magnification view of the end of the lever, showing the position of the tip (at the apex of the pyramid) relative to the lever. The tip is off-axis by an amount close to its nominal height of 3 micrometers, which is an additional source of coupling between normal and lateral forces.

as Sader's first order solution for the solid triangle region at the end of the lever. His analysis shows that using the actual arm width, instead of the arm width projected in the y direction, is a better approximation for the normal force constant. Sader's analysis also shows that values for the normal force constant estimated by good PBA-type approximations are within 10-20% of the results of a detailed finite element calculation. The errors resulting from the approximations used in the force estimates are probably less than the errors due to uncertainty in the physical properties of the lever (thickness, modulus, tip height, metalization thickness, etc.).

The results of this calculation for a Park Scientific Instruments "F" lever that is displayed in Figure 3.2 are shown in Figure 3.3, assuming an elastic modulus of 155 GPa and a Poisson ratio of 0.27 for CVD silicon nitride[5]. If the laser beam is positioned in the center of the triangular region at the end of the lever, the estimated angular deflections

produced by normal, lateral and buckling forces are 32.2, 1.26 and 1.99 μrad/nN, respectively. For this relatively short and stiff lever, the triangular fillets increase the normal stiffness by ~10%. Integrating the expressions for angular deflection a second time, we obtain estimates for the force constants of 0.508, 132 and 209 N/m. The nominal normal force constant for the "F" lever is 0.50 N/m. These calculation have not taken the tip offset into account (Figure 3.2), nor the effect of the gold coating.

The sensitivity ratio $R_{LEVER}(x)$ is plotted in Figure 3.3(b). This graph shows that R_{LEVER} is about 20% more sensitive to laser spot position for the "V" lever than for the simple beam of the same length and tip height. This is because the triangle at the end of the "V" lever twists more than any other part, while most of the bending takes place near the base of the cantilever, where the normal force lever moment is the greatest.

For any of these calculations, all the cantilever dimensions and the relevant moduli of elasticity (Young's modulus, shear modulus, Poisson's ratio) are needed to calculate the force constants. The density is also needed to calculate the resonance frequency, which is a useful comparison because the free resonance frequency of these cantilevers is typically very easy to measure from the power spectrum of the cantilever's thermal vibrations. Such a measurement reduces the number of unknowns in the calculations[15]. In any event, the dimensions of the cantilevers are not easy to measure (a good scanning electron microscope is required, particularly to measure the sub-micrometer thickness of the cantilever which is a critical parameter), and the elastic moduli and density of the cantilever materials are uncertain.

3.4 Normal Force Calibration

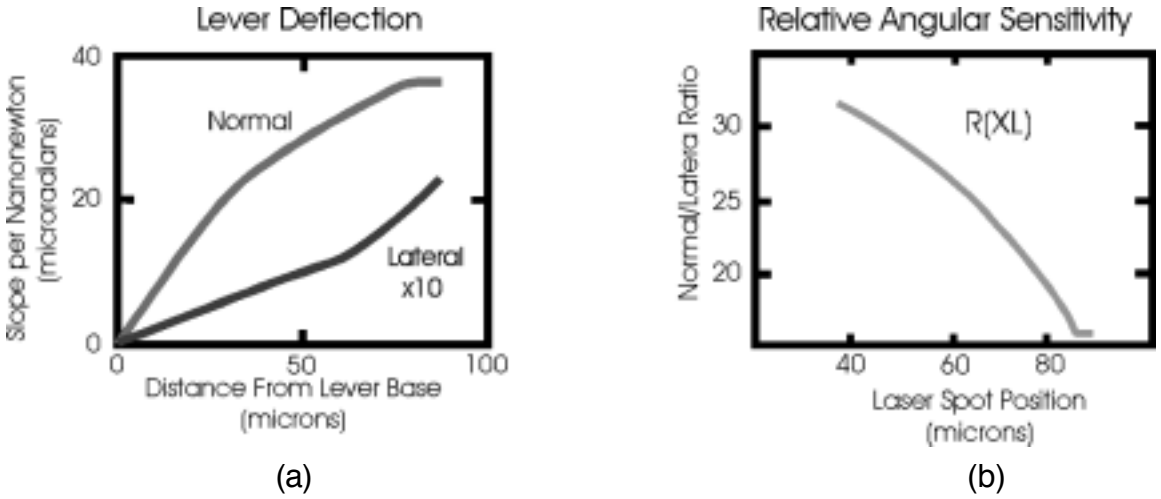

Figure 3.3 (a) Calculated curves showing the variation in slope (in micro-radians) along the length of the triangular region at the end of the cantilever shown in Figure 3.2 for a 1 nN normal or lateral force (lateral slope x10). (b) The ratio of angular deflections for this lever in response to normal and lateral forces, as a function of the laser spot position. A ~10 μm uncertainty in laser spot position will give a 20% variation in measured friction coefficient.

While these formulae and calculations are useful to obtain estimates of the forces applied, clearly from the above discussion it is much more desirable to have an *in-situ* method of directly measuring cantilever force constants. Unfortunately, since the microfabricated levers are so small, non-destructive *in-situ* testing is difficult. Nonetheless, some methods for calibration of the normal force constant have been successfully implemented. These include: measuring deflections or resonance frequency shifts for levers loaded with known masses[16-18], and measuring the deflection of the cantilever when in contact with another lever of known spring constant[19,20]. Comparison of the cantilever's thermal noise with formulae can provide a calibration[21] although measurements of the cantilever's properties are still required. It is incorrect to use formulae which regard the cantilever as a point mass on the end of a massless spring, as was done in one paper[22]. Currently, most AFM work has estimated forces from calculations like those mentioned above[15], including the work discussed in this thesis.

3.5 Lateral Force Wedge Calibration

In this section we describe an *in-situ* method of experimentally measuring the combined response of the lateral force transducer (the cantilever/tip combination) and the deflection sensor. Our method is based on comparing lateral force signals on surfaces with different slopes. The known geometrical contribution to the total lateral force, *i.e.* the product of the applied load and the tangent of the slope, gives a direct calibration of lateral force response in terms of the normal force response. If the normal force constant is known, then completely quantitative friction measurements can be made. Even if the normal force constant is uncertain, the ratio of normal to lateral forces can be determined quantitatively. An experimental force calibration is made by sliding the tip across a surface of known slope and measuring the lateral force signal as a function of applied load.

In principle, this could be carried out on any surface that is tilted with respect to the lateral scanning direction. In practice, this is difficult to realize because (a) if the surface is tilted by the experimenter, there will be some uncertainty in the tilt angle, (b) we will show that to accurately calibrate the lateral force response, *two* surfaces of different tilt angles must be used and (c) it may not be possible to contact the tip to a tilted surface without the surface touching the side of the cantilever chip or its holder, since microfabricated cantilever tips are usually very short.

These problems are resolved by using the faceted $SrTiO_3$ (305) surface proposed by Sheiko *et al.*[23] as a measure of tip sharpness. When annealed in oxygen, $SrTiO_3$ (305) facets into a (101) and (103) planes which form extended ridges along the [010] direction. The (101) and (103) planes are respectively tilted -14.0° and +12.5° with respect to the original (305) surface. The ridges are typically 5 to 20 nm high and are spaced 10 to 100 nm apart (Figure 3.4). We thus have a test sample that provides two sloped surfaces with exactly known relative angles. Furthermore, as demonstrated by Sheiko *et al.*, the top of the $SrTiO_3$ ridges are extremely sharp, and a topographic AFM scan over the ridge produces an

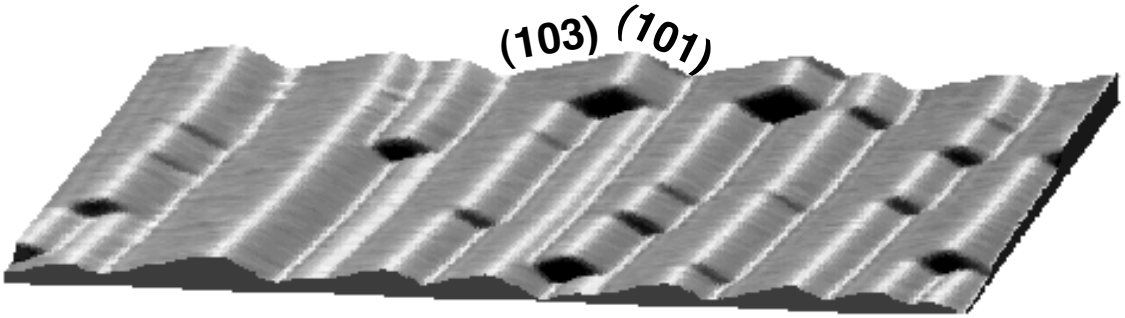

Figure 3.4 A 410 nm x 410 nm topographic AFM image (light shaded) of the $SrTiO_3$ surface showing (103) and (101) facets. The apparent rounding of the ridge crests is due to the ~40 nm radius of the AFM tip used for this image. The widest facets are used to measure lateral signals as a function of load for the cantilever lateral force calibration.

image of the tip. This is also quite important, as accurate knowledge of the tip shape is also required for quantitative FFM experiments[24].

The wedge method has some additional advantages. It can be used to determine the absolute orientation of the sample while confirming the microscope Z calibration. Even though the angle between the two $SrTiO_3$(305) facets is known, the average surface normal may be tilted by a small angle relative to the microscope Z axis. Calibrating the AFM XY displacement is usually not too difficult. Crystal lattices can be used for nanometer scale standards, and lithographically patterned standards work on the μm scale. We calibrate Z displacement in terms of XY displacement by making a topographic image of the $SrTiO_3$ sample, and adjusting Z until the angle between the facets is 26.5°. Now that XY and Z are calibrated, the overall slope of the surface can be directly determined from the image (in practice we solve for the slope and Z calibration simultaneously, see the appendix for details).

To get an accurate force calibration with the wedge method, the tip must slide across one facet for a reasonable distance before reaching the next facet or ridge crest. This is not possible unless $2R_{tip}\sin\theta$ is significantly smaller than the spacing between ridge crests. It

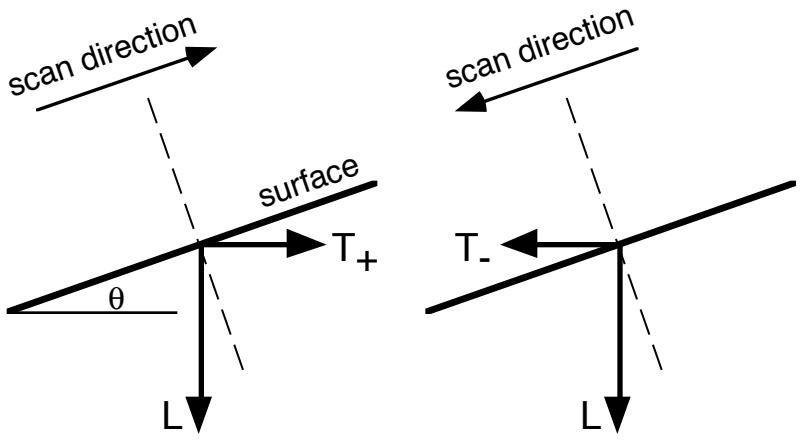

Figure 3.5 Forces exerted on the surface by the AFM tip while scanning up or down a sloped surface.

is difficult to calibrate tips with radii greater than ~ 100 nm even using the widest facets on our $SrTiO_3$ sample. The procedure is straightforward for tip radii ~ 50 nm or less. It may be possible to prepare a similar sample with larger facets for calibrating blunt tips.

3.6 Wedge Calculations

The vector diagrams in Figure 3.5 show the forces acting on the end of the tip while scanning up or down a sloped surface. The two forces applied by the tip on the surface, the vertical load L (down is positive) and the horizontal tractive force T (right is positive) must be balanced by a reaction force from the surface acting on the tip. This can be divided into two components, a friction component F_f parallel to the surface and a second component N normal to the surface. When the tip slides across the surface, these forces are in equilibrium. At a given load, the tractive force, friction and normal forces depend on the direction of motion, so

$$N_{\pm} = L\cos\theta \pm T_{\pm}\sin\theta \tag{3.19}$$

$$F_f(N_{\pm}) = T_{\pm}\cos\theta \mp L\sin\theta \tag{3.20}$$

In these equations '+' denotes uphill motion and '-' downhill motion. N, L and T are signed quantities, while F_f is the positive magnitude of the frictional force acting against the direction of motion.

We experimentally measure the voltage output from the lateral force transducer T_o where $\alpha T_o = T$ (the 'o' subscript will be used to indicated a force measured in transducer output volts rather than Newtons). If we can find α (Newtons per volt) we have a direct calibration of the lateral force response of the FFM. The calibration constant α is a product of all the factors of the experiment - the lever lateral force constant, the deflection of the reflected laser beam as a function of lateral tip displacement, and the photodiode angular sensitivity. This method will work equally well for other types of lateral force transducers, including optical interferometry and piezoresistive detection.

To solve the calibration problem we need a functional form for the frictional force $F_f(L)$. This can be an empirical fit from measuring friction on a flat surface, or a theoretical form from the Hertz or JKR theories[24]. These shall be discussed in detail in Chapter 5. Tip-surface adhesion usually has a significant effect on $F_f(L)$ in FFM experiments. When friction is linearly dependent on load, adhesion is often treated as a force offset. We find experimentally that the friction-load relation for silicon or silicon nitride tips on the strontium titanate surface in air is well represented by a linear form $F_f(N_\pm) = \mu \bullet (N_\pm + A)$ where A is the adhesion or pull-off force. In this case

$$N_+ = \frac{L + \mu A \sin\theta}{\cos\theta - \mu \sin\theta} \tag{3.21}$$

and

$$N_- = \frac{L - \mu A \sin\theta}{\cos\theta + \mu \sin\theta} \tag{3.22}$$

Note that the normal force depends on the friction and on the direction of motion.

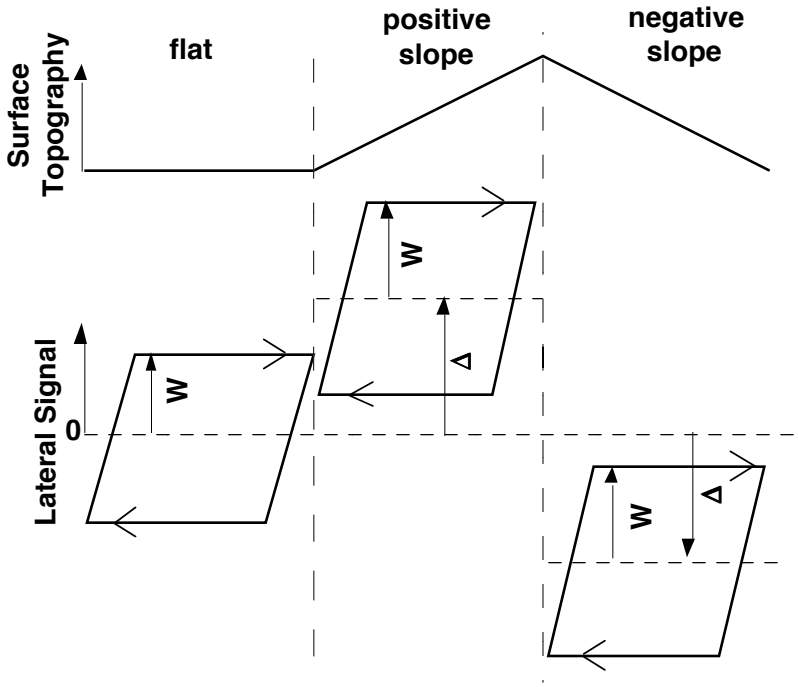

Figure 3.6 Schematic "friction loops" (lateral signals for back and forth scans) for flat, positively sloped and negatively sloped surfaces at the same applied load. The friction loop half-width W is slightly different for the three cases, while the loop offset Δ is substantially different and is indicative of the overall tilt of each surface. The values of W and Δ are measured over a range of applied loads for known slopes and used to calibrate the lateral force response of the cantilever.

On a flat surface, the "frictional force" is determined by taking half the difference between the left-to-right and right-to-left lateral deflection forces, *i.e.* the half width of the friction loop $W(L)$. In this case, since the surface is tilted, the effective load is direction-dependent, and the expression for $W(L)$ is more complicated. Furthermore, the offset of the friction loop $\Delta(L)$ is not zero and depends on load. This is illustrated in Figure 3.6, where bi-directional lateral force loops are drawn for flat, positively tilted, and negatively tilted surfaces respectively and the measured quantities W_o and Δ_o are indicated.

Experimentally, we measure lateral forces for a range of applied loads, and use the slopes $\Delta' \equiv \partial\Delta/\partial L$ and $W' \equiv \partial W/\partial L$ in calculations, which are independent of L due to the

assumption of linearity. This eliminates the pull-off force from the equations, as well as any DC offset in the lateral force sensor. These slopes are given by:

$$\alpha\Delta'_o = \Delta' = \frac{\left(1+\mu^2\right)\sin\theta\cos\theta}{\cos^2\theta - \mu^2\sin^2\theta} \tag{3.23}$$

and

$$\alpha W'_o = W' = \frac{\mu}{\cos^2\theta - \mu^2\sin^2\theta} \tag{3.24}$$

In the limiting cases of no friction, $\Delta' \rightarrow \tan\theta$ and $W' \rightarrow 0$, and for no slope $\Delta' \rightarrow 0$ and $W' \rightarrow \mu$ as expected. Using these two equations, we can calculate the tip-surface friction coefficient and lateral force calibration constant. The ratio of these expressions gives μ:

$$\mu + \frac{1}{\mu} = \frac{2\Delta'_o}{W'_o \sin 2\theta} \tag{3.25}$$

From the form of this expression, there is an ambiguity in the problem, since μ and $1/\mu$ are equally good mathematical solutions which give different results for α. This ambiguity may be resolved by choosing the appropriate root using an estimate for α from the type of calculation described in section 3.3, or if μ is known to be less than one. Once μ is determined, α can be found from the equations defining W' or Δ'. Experimentally, it is best to solve for α using data from two different slopes, as discussed below.

3.7 Experimental Difficulties

In the ideal case the lateral force response of the cantilever and deflection sensor has been calibrated. However there can be significant "cross talk" between normal and lateral cantilever deflections. As discussed above, the response of the optical beam FFM deflection sensor is 20-80 times greater for normal forces than for lateral forces. In addition, the

normal forces are often larger than the lateral forces. A small misalignment of the laser or cantilever with respect to the quadrant photodiode, for example a rotation of the photodiode by ~ 2°, can mean that the normal force contribution to the lateral deflection output is as large as the lateral force contribution. In normal FFM experiments this problem is avoided by measuring friction loop width, or $W(L)$, since the "cross talk" primarily effects the friction loop offset $\Delta(L)$. Cross talk is a concern in the wedge calibration experiment since the lateral force offset $\Delta(L)$ is important in the calibration calculation.

In our experiment, we compensate for the cross talk electronically, by adding or subtracting a fraction of the normal force output from the lateral force output. The compensation is adjusted by taking an approach curve, or by oscillating the cantilever out of contact with the surface, where there should be no "real" lateral forces, and adjusting the compensation to null the lateral force output. Such compensation is also available on some commercial FFM electronics[25]. Even with careful compensation, the residual cross talk may be too large to neglect in the calibration calculations.

The effect of cross talk can be minimized by measuring Δ_0' and W_0' on the (103) and (101) facets of the $SrTiO_3$ surface and then using $\Delta_0'(103)$-$\Delta_0'(101)$, $W_0'(101)$ and $W_0'(103)$ for the calibration calculation. These quantities all involve *differences* between lateral signals for the same applied load, so cross talk has been subtracted out to first order. The details of the two-slope calibration are given in the Appendix.

The above discussion has assumed that the applied load L is known. Since the direct experimental calibration of normal spring constants is also difficult, in some cases only an experimental signal L_o proportional to the normal load, $L = \beta L_o$, is known. In this case it is not possible to get the absolute lateral force calibration, but only

$$R_{DETECTOR} \bullet R_{LEVER}(X_{LASER}) = \alpha/\beta. \qquad (3.26)$$

It is still possible to get the friction coefficient μ if friction is proportional to load, since on a flat surface $\mu = R_{DETECTOR} \bullet R_{LEVER}(X_{LASER}) \bullet T_o/L_o$. It is not sufficient to assume that the voltage

applied to the Z piezo is proportional to load, since there are significant non-linearities in piezo response, which depend on the speed and direction of displacement[26-28].

3.8 Experimental Lever Calibration

For the following example, we have not calibrated the normal force constant of the cantilever. Therefore, we will actually take derivatives of the experimentally measured quantities Δ_0 and W_0 with respect to L_0, the experimental load signal in output Volts. Thus, $\Delta_0' \equiv \partial\Delta/\partial L_0$ and $W' \equiv \partial W/\partial L_0$. In this case, equations (3.23) and (3.24) become

$$\alpha/\beta \cdot \Delta_o' = \Delta' = \frac{\left(1+\mu^2\right)\sin\theta\cos\theta}{\cos^2\theta - \mu^2\sin^2\theta} \tag{3.27}$$

and

$$\alpha/\beta \cdot W_o' = W' = \frac{\mu}{\cos^2\theta - \mu^2\sin^2\theta} \tag{3.28}$$

We have thus used the wedge calibration procedure described with our AFM to measure α/β for cantilevers of three different nominal spring constants. In this system the laser beam is carried by a single-mode fiber and well-focused on the cantilever, so $R_{DETECTOR} \approx 1$[4]. The cantilevers are "V"-shaped silicon nitride "Sharpened Microlevers" from Park Scientific Instruments[29]. The levers are gold coated, and the pyramidal tips are etched back to get a sharp tip with a nominal radius of ≈ 30 nm. We made measurements on the "*D*", "*E*" and "*F*" levers which have nominal normal force constants 0.03, 0.10 and 0.50 N/m. Two different *E* levers from the same wafer were analyzed.

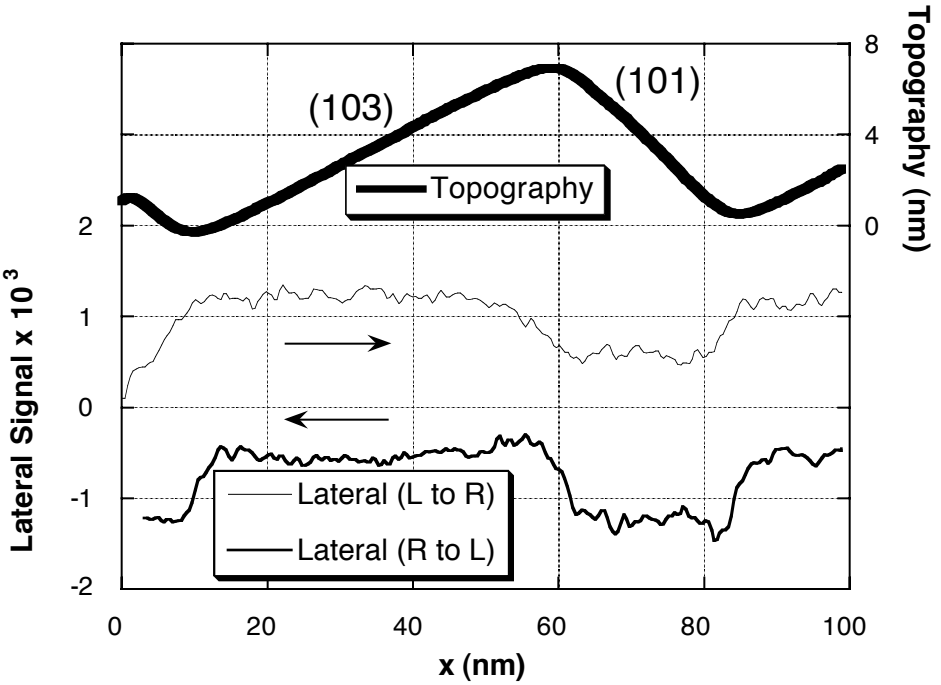

Figure 3.7 Experimental lateral deflection signals T_o (1-2/A+B) measured on the (101) and (103) facets of the $SrTiO_3$(305) surface for each direction at a given load. The simultaneously acquired topography (thick line) is also shown. W(L) and Δ(L) are calculated from this data. The complete series of measurements over a range of loads is shown in Figure 3.8.

The $SrTiO_3$ sample was aligned so that the ridges were perpendicular to the lateral scanning direction. The lateral and normal bending signals were recorded as the tip scanned back and forth over both facets of a single ridge. The feedback was active so that each line scan across the sloped surface was recorded at the same externally applied load. After each line was recorded, the feedback set point (applied load) was increased under computer control, and another line scan acquired. 256 line scans of 256 points were recorded in each data set. The average value of the subset of points for each facet was calculated for each load. Figure 3.7 shows an example of unprocessed data from a single line scan (friction

loop), showing the simultaneous topography and lateral deflection signals for both scanning directions.

A plot of lateral force *vs*. load, obtained in this case with an *E* lever, is shown in Figure 3.8. Figure 3.8(a) shows the lateral bending signals (left-to-right and right-to-left) plotted vs. the normal bending signal for both facets. Figure 3.8(b) shows the resulting friction loop width and offset plotted vs. the normal bending signal (load) for both facets, with linear fits to the data. As predicted in section 3.7, the slopes $W_0'(101)$ and $W_0'(103)$ are similar, while $\Delta_0'(101)$ and $\Delta_0'(103)$ reflect the change in sign of the tilt angle. The data deviates slightly from nonlinearity, although the linear fit results in at most a 3.5% statistical uncertainty in the slopes for a given measurement. A more complex fit than the simple linear fit utilized could be slightly more accurate, but would complicate the method substantially as equations (3.21) and beyond would need to be modified.

The two-slope wedge equations in the appendix were used to calculate α/β. We did not have a good experimental value for the lever normal force constant, so we report α/β instead of the absolute lateral force response α. The results are summarized in Table 3.1.

Figure 3.8 (following page) (a) Lateral deflection signals for left-to-right and right-to-left scanning directions (1-2/A+B) as a function of load deflection signal (A-B/A+B) for the (101) and (103) facets. The total A+B signal (photodiode current) was 185 μA. (b) The friction loop width W(L) and offset Δ(L) as a function of load for the (101) and (103) facets. Straight lines fit the data very well, justifying our assumption of linear friction behavior. The slopes of each line are measured and used in formulae given in the appendix to solve for α/β, the normal force to lateral force deflection ratio.

(a)

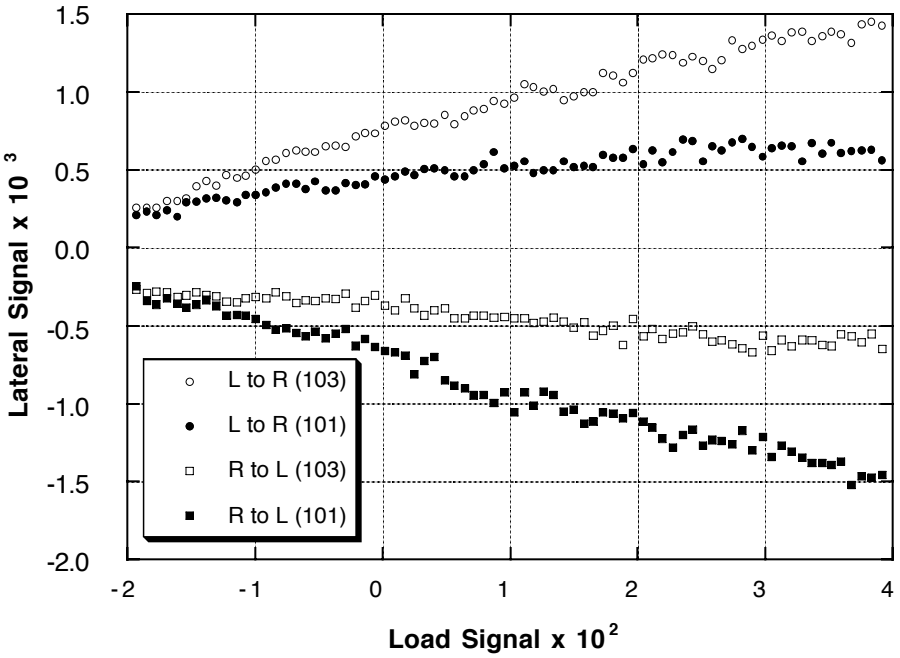
Lateral Signal x 10 3
Load Signal x 10 2
L to R (103)
L to R (101)
R to L (103)
R to L (101)
1.5
1.0
0.5
0.0
-0.5
-1.0
-1.5
-2.0
-2
-1
0
1
2
3
4

(b)

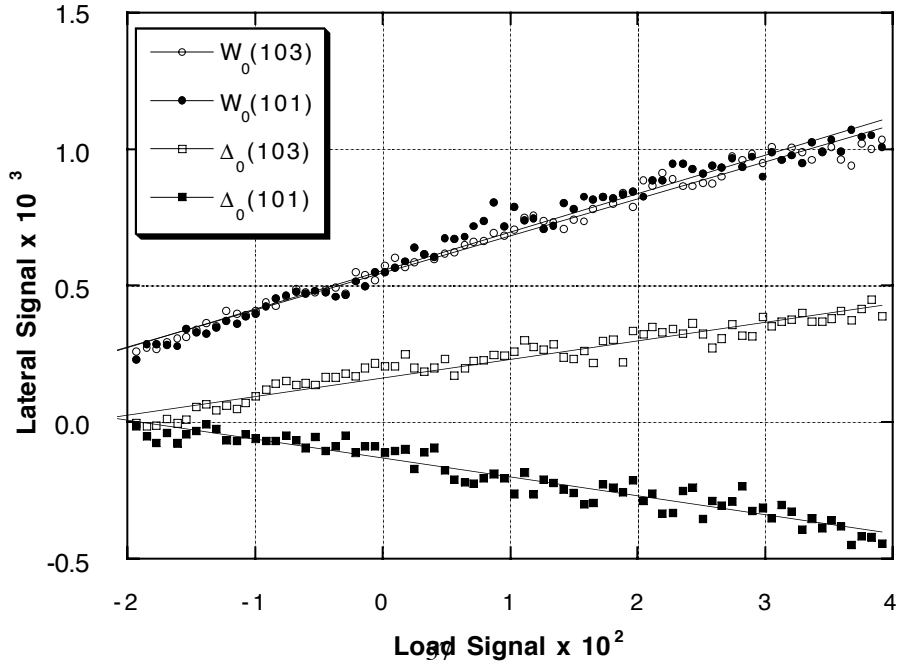
Lateral Signal x 10 3
Load Signal x 10 2
W0(103)
W0(101)
Δ0(103)
Δ0(101)
1.5
1.0
0.5
0.0
-0.5
-2
-1
0
1
2
3
4

The α/β values are averages of several data sets, each acquired on a different ridge. For comparison, the table includes the spring constants estimated by the method of section 3.6, and the value for R_{LEVER} assuming that X_{LASER} was located in the center of the solid triangular region at the end of the lever (Figure 3.2). Some data sets were recorded on different days. The error quoted is the statistical variation. Since, for our instrument, $R_{DETECTOR} \approx 1$, then from equation (3.26) , $\alpha/\beta \approx R_{LEVER}$. We see from the results that the experimental α/β values are generally consistent with the R_{LEVER} values estimated from material properties, but the difference is not insignificant. The experimental friction coefficients tend to be slightly higher for the (103) facet of strontium titanate relative to the (101) facets. We noted more substantial variations in friction coefficients from day to day. As mentioned, these experiments were carried out in air with no humidity control. Friction coefficients on other materials measured with AFM have been observed to vary with relative humidity[30,31]. This may partially account for the variation of friction coefficients observed. Friction coefficients may also vary from lever to lever due to changes in tip radius.

There are some subtle experimental requirements for successful application of this method. As stated before, the method will fail if the tip is too blunt as the tip will always be riding over the sharp ridges, instead of scanning on the facets. Generally a tip radius of 50 nm or less is required. Careful examination of the topographic image can verify if the tip is sufficiently sharp. Specifically, taking the numerical derivative of the topographic data perpendicular to the $SrTiO_3$ ridges will reveal if a constant slope is measured on the facets. This is the signature of the tip's contact with the flat facets as opposed to the sharp ridge.

Another problem can arise if the facet where one is scanning contains any contamination or a step. One can see in Figure 3.3 that the (101) facet often possesses small steps which can be difficult to perceive. One muse acquire a topographic image first to identify a locally flat pair of facets for the measurement.

Table 3.1 Experimental lever calibration results and estimates based on calculations.

	EXPERIMENTAL			ESTIMATE D		
LEVER	μ_{101}	μ_{103}	α/β	R_{LEVER}	k_{NORMAL}	$k_{LATERAL}$
D (0.03)	.42±.10	.51±.09	51±6	61.6	.037	66.6
E#1 (0.1)	.50±.05	.52±.05	43±3	39.4	.111	92.7
E#2 (0.1)	.66±.14	.74±.12	36±4	39.4	.111	92.7
F (0.5)	.33±.02	.41±.03	19±1	25.5	.508	132

3.9 Error Analysis

We have considered the propagation of errors for this calibration method. For a given uncertainty in the experimentally measured slopes $W_0'(101)$, $W_0'(103)$, $\Delta_0'(101)$, and $\Delta_0'(103)$, the uncertainty in α/β will depend upon the value of μ on each facet. μ apparently changes for different tips and different relative humidities. To facilitate this analysis, let us assume that $\mu_{101} = \mu_{103} \equiv \mu$. In general it is expected that the uncertainty will be smaller when μ is smaller since the measured signals are due more to geometry than friction, and it is this geometrical coupling that is leading to the calibration.

In Figure 3.9, we graph the experimental error in α/β as a function of μ for 1%, 3%, 5% and 10% uncertainty in the slope measurements. At low μ, the uncertainty approaches

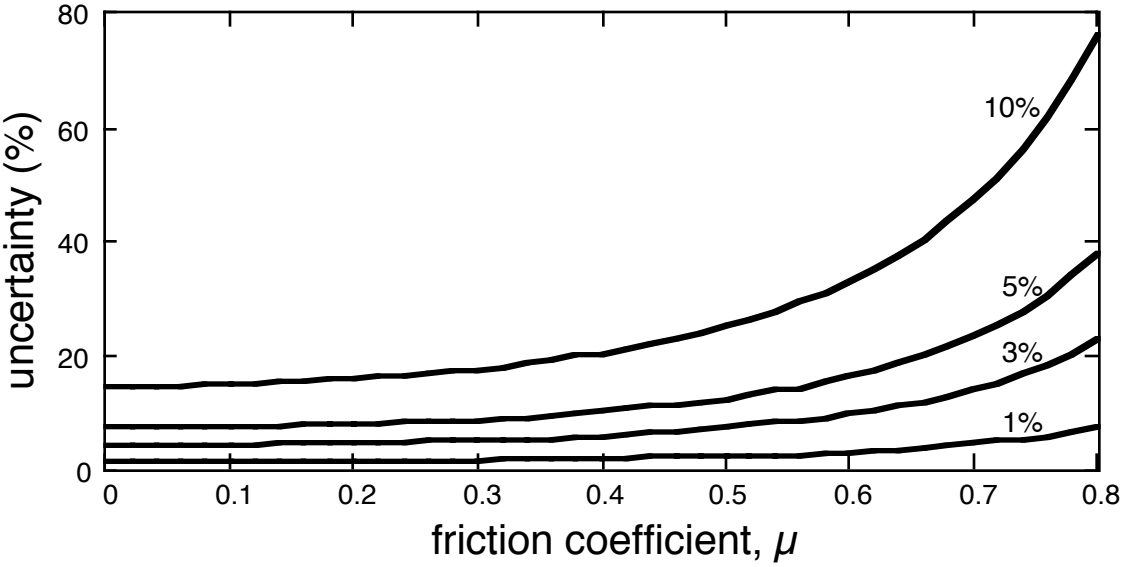

Figure 3.9 Uncertainty in the measurement of α/β as a function of the friction coefficient μ (for simplicity we assume that $\mu_{101} = \mu_{103}$). The error is calculated assuming the measurement errors in W_0' and Δ_0' for both facets is 1%, 3%, 5% and 10% respectively.

the fundamental limit, as expected. The error diverges for large μ since the sensitivity to geometry is overwhelmed by the friction signal.

This calculation indicates that low friction is clearly desirable for this calibration method. Furthermore, we see that errors become unreasonable for $\mu > 0.7$. For most of the measurements performed, friction between tips and the $SrTiO_3$ sample is generally low enough for accurate measurements. Future work should attempt to measure μ as a function of relative humidity, to see which experimental conditions are optimal for the experiment.

3.10 Summary

We have demonstrated a quantitative method of lateral force calibration for the microfabricated tip-cantilever assemblies used in friction force microscopy. We find that there are significant variations among cantilevers fabricated from the same wafer. Tip variations also play a role. Furthermore, the overall system calibration depends on the precise alignment of the deflection sensor where optical detection is used.

In order to perform quantitative frictional force microscopy with the atomic force microscope, it is important to perform an experimental force calibration for *each* cantilever sensor.

3.11 Appendix

3.11.1 Photodiode Response

An elliptical Gaussian beam has a normalized intensity distribution

$$\Gamma(y,z) = \frac{2}{\pi \Delta\omega_y \Delta\omega_z} e^{\frac{-2y^2}{\Delta\omega_y^2} + \frac{-2z^2}{\Delta\omega_z^2}} \tag{3.29}$$

Here $\Delta\omega$ is the angular half width of the *field* distribution, following the conventions of Gaussian optics. The half width of the intensity distribution is then $\Delta\omega/\sqrt{2}$. If the beam is deflected by d in the y direction, the signal is given by

$$S(d) = \frac{A-B}{A+B} = 1 - \frac{1}{\Delta\omega_y}\sqrt{\frac{8}{\pi}}\int_d^\infty e^{\frac{-2y^2}{\Delta\omega_y^2}} dy \tag{3.30}$$

The integral

$$I(d) = \int_d^\infty e^{\frac{-2y^2}{\Delta\omega_y^2}} dy = \int_0^\infty e^{\frac{-2(t+d)^2}{\Delta\omega_y^2}} dt \tag{3.31}$$

can be expanded around $d = 0$ by taking a derivative

$$\frac{dI}{dd} = \int_0^\infty \frac{\partial}{\partial d}\left[e^{\frac{-2(t+d)^2}{\Delta\omega_y^2}} \right] dt = \int_0^\infty -\frac{4(t+d)}{\Delta\omega_y^2} e^{\frac{-2(t+d)^2}{\Delta\omega_y^2}} dt = -e^{\frac{-2d^2}{\Delta\omega_y^2}} \tag{3.32}$$

likewise higher derivatives can be calculated

$$\frac{d^2 I}{dd^2} = \frac{4d}{\Delta\omega_y^2} e^{\frac{-2d^2}{\Delta\omega_y^2}} \tag{3.33}$$

and

$$\frac{d^3 I}{dd^3} = \left[\frac{4}{\Delta\omega_y^2} - \frac{16d^2}{\Delta\omega_y^4} \right] e^{\frac{-2d^2}{\Delta\omega_y^2}} \tag{3.34}$$

When these derivatives are evaluated at $d = 0$, the even terms vanish, as expected, since $S(d)$ is an odd function. Finally we put these terms into a Taylor expansion and get

$$S(d) = \sqrt{\frac{8}{\pi}} \frac{d}{\Delta\omega_y} \left[1 - \frac{4}{3!}\left(\frac{d}{\Delta\omega_y}\right)^2 + \frac{48}{5!}\left(\frac{d}{\Delta\omega_y}\right)^4 - \frac{960}{7!}\left(\frac{d}{\Delta\omega_y}\right)^6 + \ldots \right] \tag{3.35}$$

3.11.2 Z Calibration and Tilt Measurement

A measurement of the apparent topography of the $SrTiO_3$ sample slopes provides a check of the relative Z:X piezo calibration, as well as determining the overall tilt of the sample with respect to the scanning plane. This is important because one must use the actual physical angles between the sloped facets and the scanning plane in the wedge calculations.

We assume that the X calibration of the piezo scanner is correct and that the initial Z calibration is approximate. We acquire a topographic image of the faceted strontium titanate surface, with known facet angles of $\theta_1 = -14.0°$ and $\theta_2 = 12.5°$ relative to the (305) plane. We wish to determine the correction factor γ for the Z calibration such that $Z_{TRUE} = \gamma \bullet Z_{INITIAL}$ and the macroscopic tilt angle ψ of the (305) surface relative to the scanning plane, projected onto the *y*-*z* plane.

From the image we measure the apparent slopes ($\Delta Z/\Delta X$) of the facets S_1 and S_2. Then $\tan(\theta_1 + \psi) = \gamma \bullet S_1$ and $\tan(\theta_2 + \psi) = \gamma \bullet S_2$. From this we make a quadratic equation

$$\tan(\theta_1 - \theta_2) = \frac{\gamma S_1 - \gamma S_2}{1 + \gamma^2 S_1 S_2} \tag{3.36}$$

Solving for γ gives positive and negative solutions. The positive solution is physically reasonable:

$$\gamma = \frac{(S_1 - S_2) - \sqrt{(S_1 - S_2)^2 - 4 S_1 S_2 \tan^2(\theta_1 - \theta_2)}}{2 S_1 S_2 \tan(\theta_1 - \theta_2)} \tag{3.37}$$

Then the tilt angle is easily calculated: $\gamma = \tan^{-1}(\gamma \bullet S_1) - \theta_1$.

3.11.3 Two Slope Calibration

We wish to find the lateral force calibration α in terms of the experimentally measured quantities $W_0'(101)$, $W_0'(103)$, $\Delta_0'(101)$, and $\Delta_0'(103)$. This discussion assumes these derivatives are taken with respect to the calibrated load L. If the load is not calibrated, then these derivatives are taken with respect to the load signal L_0, and thus α is replaced by α/β in equations (3.40) and (3.44).

Since the magnitude and offset of lateral force coupling is unknown, we use the difference $\Delta_0'(101) - \Delta_0'(103)$ in calculation. The ratios of uncalibrated experimental values should be equal to the ratios of the forces as calculated from geometry in section 3.6. Therefore

$$p \equiv \frac{W_o'(101)}{W_o'(103)} = \frac{W'_{101}}{W'_{103}} \tag{3.38}$$

$$q \equiv \frac{\Delta_o'(103) - \Delta_o'(101)}{W_o'(101)} = \frac{\Delta'_{103} - \Delta'_{101}}{W'_{101}} \tag{3.39}$$

$$\alpha = \frac{W'_{103}}{W_o'(103)} \tag{3.40}$$

Here p and q are pure number ratios derived from experimental data such as that in Figure 3.8. From (3.38) and the equations in section 3.6:

$$\mu_{101} = \frac{-1 + \sqrt{1 + \kappa^2 \sin^2 2\theta_{101}}}{2\kappa \sin^2 \theta_{101}} \tag{3.41}$$

$$\kappa \equiv p \frac{\mu_{103}}{\cos^2 \theta_{103} - \mu_{103}^2 \sin^2 \theta_{103}} \tag{3.42}$$

Here, θ_{101} and θ_{103} represent the physical angles of each facet with respect to the scanning plane, *i.e.* $\theta_{101} = -14^\circ + \psi$, and $\theta_{103} = 12.5^\circ + \psi$.

There is a also an ambiguity here between a friction coefficient and its reciprocal, similar to the one slope solution of section 3.6. We choose the quadratic roots giving $\mu < 1$, which gives calibration results consistent with the calculated lever properties. Equation (3.42) expresses μ_{101} in terms of μ_{103}. From (3.39),

$$2q = \left(\frac{1}{\mu_{103}} + \mu_{103}\right) \sin 2\theta_{103} \frac{1}{p} - \left(\frac{1}{\mu_{101}} + \mu_{101}\right) \sin 2\theta_{101} \tag{3.43}$$

Now we can substitute (3.41) and (3.42) into (3.43) to eliminate μ_{101}. As the resulting expression is difficult to invert, we solve it numerically for the root such that $0 < \mu_{103} < 1$. With this solution, we find the calibration

$$\alpha = \frac{1}{W_o'(103)} \frac{\mu_{103}}{\cos^2 \theta_{103} - \mu_{103}^2 \sin^2 \theta_{103}} \tag{3.44}$$

Chapter 3 References

[1] G. Meyer and N. Amer, Appl. Phys. Lett. **57,** 2089 (1990).

[2] O. Marti, J. Colchero, and J. Mlynek, Nanotechnology **1,** 141 (1991).

[3] W. F. Kolbe, D. F. Ogletree, and M. B. Salmeron, Ultramicroscopy **42-44B,** 1113 (1992).

[4] Q. Dai, R. Vollmer, R. W. Carpick, D. F. Ogletree, and M. Salmeron, Rev. Sci. Instrum. **66,** 5266 (1995).

[5] Dr. M. Tortonese, Park Scientific Instruments Inc., Sunnyvale, CA (personal communication).

[6] Dr. R. Alley, Berkeley Sensors Group, Berkeley, CA (personal communication).

[7] J. E. Sader, I. Larson, P. Mulvaney, and L. R. White, Rev. Sci. Instrum. **66,** 3789 (1995).

[8] J. E. Sader and L. R. White, J. Appl. Phys. **74,** 1 (1993).

[9] J. M. Neumeister and W. A. Ducker, Rev. Sci. Instrum. **65,** 2527 (1994).

[10] U. D. Schwarz, P. Koster, and R. Wiesendanger, Rev. Sci. Instrum. **67,** 2560 (1996).

[11] D. F. Ogletree, R. W. Carpick, and M. Salmeron, Rev. Sci. Instrum. **67,** 3298 (1996).

[12] S. P. Timoshenko and J. N. Goodier, *Theory of Elasticity* (McGraw Hill, New York, 1987).

[13] J. E. Sader, Rev. Sci. Instrum. **66,** 4583 (1995).

[14] R. J. Warmack, X.-Y. Zheng, T. Thundat, and D. P. Allison, Rev. Sci. Instrum. **65,** 394 (1994).

[15] R. Lüthi, E. Meyer, H. Haefke, L. Howald, W. Gutmannsbauer, M. Guggisberg, M. Bammerlin, and H.-J. Güntherodt, Surf. Sci. **338,** 247 (1995).

[16] J. P. Cleveland, S. Manne, D. Bocek, and P. K. Hansma, Rev. Sci. Instrum. **64,** 403 (1993).

[17] T. J. Senden and W. A. Ducker, Langmuir **10,** 1003 (1994).

[18] A. Torii, M. Sasaki, K. Hane, and S. Okuma, Meas. Sci. Technol. **7,** 179 (1996).

[19] J. A. Ruan and B. Bhushan, Trans. ASME J. Tribology **116,** 378 (1994).

[20] Y. Q. Li, N. J. Tao, J. Pan, A. A. Garcia, and S. M. Lindsay, Langmuir **9,** 637 (1993).

[21] H. J. Butt and M. Jaschke, Nanotechnology **6,** 1 (1995).

[22] J. L. Hutter and J. Bechhoefer, Rev. Sci. Instrum. **64,** 1868 (1993).

[23] S. S. Sheiko, M. Möller, E. M. C. M. Reuvekamp, and H. W. Zandbergen, Phys. Rev. B **48,** 5675 (1993).

[24] R. W. Carpick, N. Agraït, D. F. Ogletree, and M. Salmeron, J. Vac. Sci. Technol. B **14,** 1289 (1996).

[25] RHK Inc., Rochester Hills, MI.

[26] J. Fu, Rev. Sci. Instrum. **66,** 3785 (1995).

[27] S. M. Hues, C. F. Draper, K. P. Lee, and R. J. Colton, Rev. Sci. Instrum. **65,** 1561 (1994).

[28] A. E. Holman, P. M. L. O. Scholte, W. C. Heerens, and F. Tuinstra, Rev. Sci. Instrum. **66,** 3208 (1995).

[29] Park Scientific Instruments Inc., Sunnyvale CA, USA.

[30] M. Binggeli and C. M. Mate, Appl. Phys. Lett. **65,** 415 (1994).

[31] J. Hu, X.-D. Xiao, D. F. Ogletree, and M. Salmeron, Surf. Sci. **327,** 358 (1995).